Pergamon

Acta mater. 48 (2000) 4007–4020

www.elsevier.com/locate/actamat

PREDICTING THE SIZE- AND TEMPERATURE-DEPENDENT SHAPES OF PRECIPITATES IN Al–Zn ALLOYS

S. MÜLLER[1]*, C. WOLVERTON[2], L. -W. WANG[1] and A. ZUNGER[1]

[1]National Renewable Energy Laboratory, Golden, CO 80401, USA, and [2]Ford Research Laboratory, MD3028/SRL, Dearborn, MI 48121-2053, USA

Here, σ denotes the type of ordered structure, and a_A and a_B are the equilibrium lattice constants of the bulk elements A and B

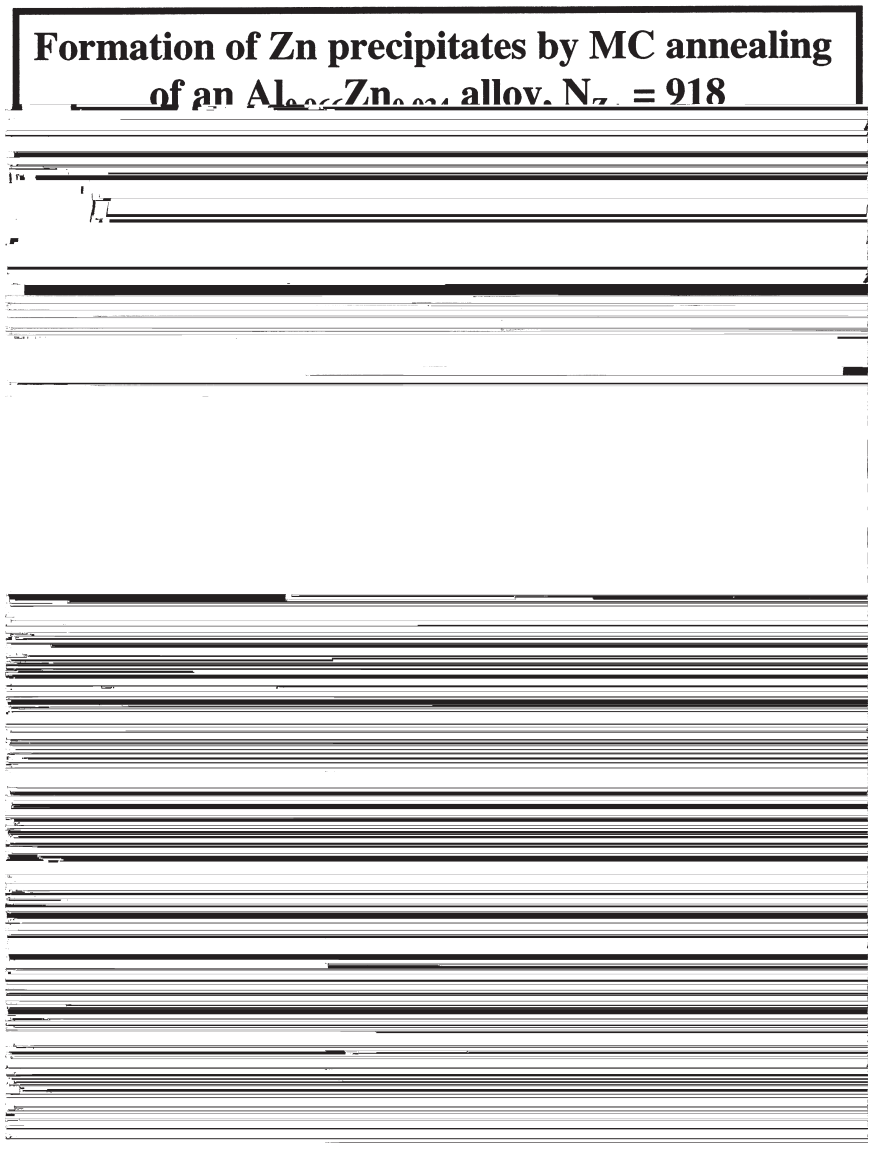

Fig. 3. Equilibrium configurations of an $Al_{0.966}Zn_{0.034}$ alloy from Monte-Carlo simulations above and below T_C, only Zn atoms are shown. Starting from a random configuration the Zn precipitate ($N_{Zn} = 918$) is formed during careful annealing below the critical temperature $T_C(x)$ given by the coherent fcc miscibility gap.

ordered Al_pZn_q compounds whose layers are oriented along the [111] direction. Consequently, we find [41] that such [111] superlattices show unusually stable formation enthalpies. For example, the Al_3Zn_3 superlattice along [111] has a formation enthalpy of only $\Delta H_f = +2.8$ meV/atom [41], while [001]-oriented structures are much higher in energy. The consequence for the formation of precipitates is now obvious: in no direction other than [111] are deformations so low in energy. Therefore, the "flattening" of precipitates in the [111] direction evident in Fig. 4 is caused by the extremely small [111] strain in Al–Zn in combination with a strong anisotropy of the chemical energy.

It is noteworthy that the c/a ratio (with respect to ideal close packing) at which the fcc Zn total energy has a minimum is practically identical to the c/a ratio in hexagonal close-packed (hcp) Zn (shown in Fig. 6 as a hexagon). Experimentally, hcp Zn has an anomalously large c/a ratio of 1.15 (with respect to ideal close packing). This anomaly of hcp Zn has been the subject of a number of earlier investigations (e.g., Refs. [59, 60]). The observation of the large c/a value in fcc Zn (Fig. 6) suggests that the physical mechanism that is responsible for the anomalous c/a ratio of hcp Zn could be the same as that causing the instability of fcc Zn. A detailed discussion about the instability of fcc Zn can be found in Ref. [41].

Fig. 4. Dependence of calculated coherent fcc Zn precipitate shape on the number of Zn atoms and temperature in Al–Zn alloys. The bottom right marks the *c*- and *a*-axes of the precipitate, which can be used for a quantitative comparison to experimental data (only Zn atoms are shown).

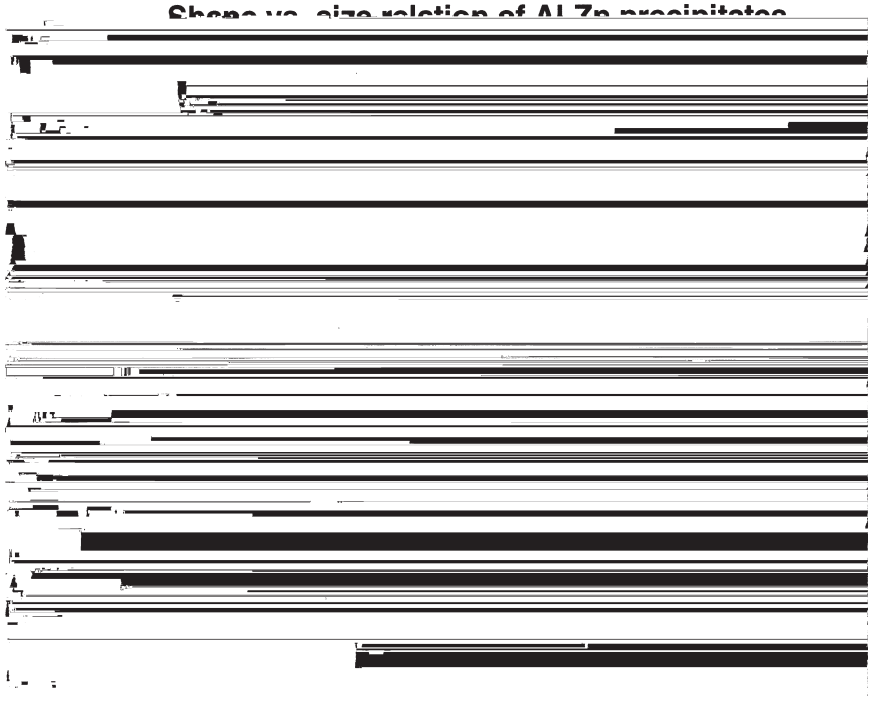

Fig. 5. Comparison of size versus shape relation of precipitates in Al–Zn between our calculations and experimental results for two different temperatures. $r_m = (ca^2)^{1/3}$ is the radius of the associated sphere having the same volume.

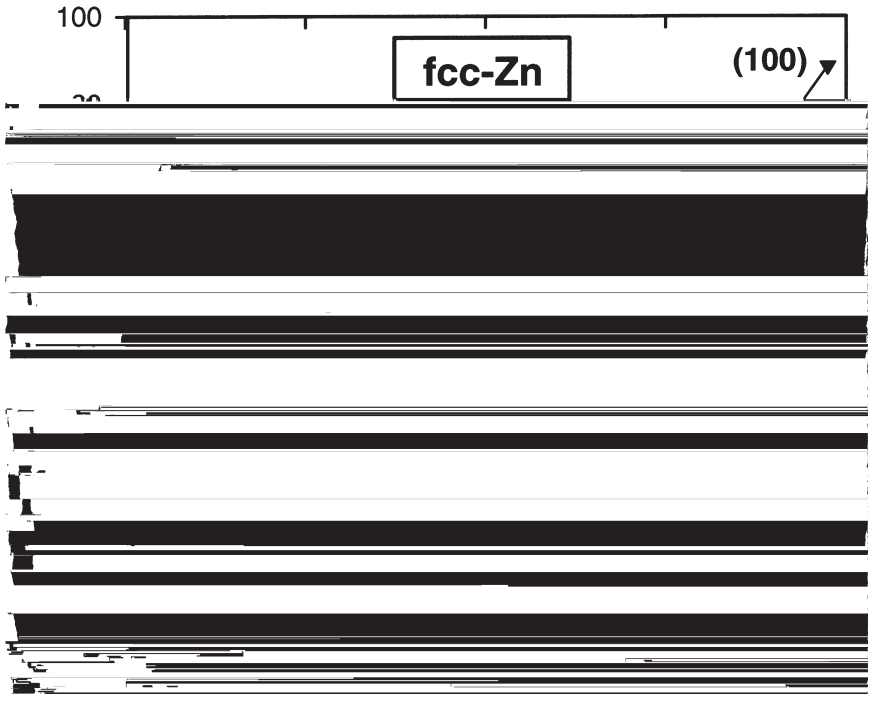

Fig. 6. Volume-conserving first-principles total energy calculations of fcc Zn deformed along the (100) and (111) directions. The energy differences caused by distortions along (100) and (111), as well as for hcp Zn, are always given with respect to the undistorted fcc lattice. The energy of hcp Zn is denoted as an open hexagon.

5. PHYSICAL ANALYSIS OF THE COMPUTATIONAL RESULTS

In order to shed light on the predicted size-dependent precipitate shape, we construct model precipitates with a *given* shape, c/a, and then evaluate their energy as function of size. Naturally, our cluster expansion Hamiltonian H_{CE} of equation (3) allows the calculation of any arbitrary given configuration at $T = 0$ K, i.e., *without* any Monte-Carlo simulations. The advantage of such an inverse approach is that the calculated energies of given shapes isolate the influence of the shape change on the energy, while the MC simulation changes the shape and the degree of order (i.e., disorder caused by finite temperature) *at the same time*, thus not allowing the effects to be separated. We chose the ideal sphere ($c/a = 1$), as well as hexagons with varying c/a ratios of 0.85, 0.50 and 0.35, as model precipitates for our calculations and determined their $T = 0$ energies for different numbers N_{Zn} of Zn atoms. The model precipitates are embedded in a $40 \times 40 \times 40$ fcc lattice cell. All sites that are not occupied by the Zn atoms, are occupied by Al atoms. So, the total number of atoms of any configuration is always 64,000. It should be mentioned that such a calculation of a formation enthalpy for a configuration consisting of 64,000 atoms does not take longer than a few seconds on a workstation or a modern PC. This short computer time for—in an atomistic sense—huge systems makes our cluster expansion a powerful tool.

Fig. 7 shows the dependence of the $T = 0$ energy of the four chosen model precipitates on their size. Only for extremely small precipitates (less than about 90 Zn atoms) does the ideal sphere ($c/a = 1.0$) represent the lowest energy at $T = 0$. With increasing size, the lowest-energy c/a ratio decreases, until at about 1600 Zn atoms the model with $c/a = 0.35$ becomes the energetically favorable shape. The transition points of the energy curves belonging to different c/a ratios are denoted in Fig. 7 by arrows. This calculation can be used to construct a step function in the size versus shape diagram, which we show in Fig. 8. For comparison, the size versus shape curve obtained via MC annealing for $T \rightarrow 0$ is also shown. It can be seen that the $T = 0$ [illegible]

éfÍ 9.943tor=/c
Fig. points s9-351(i1 -do 1 TfÍ361(a)]TJ[

$$E_{CS}(\sigma) = \frac{1}{4x\ 2\ 1}\sum_{\boldsymbol{k}} \mathrm{D}E_{eq}^{CS}(\hat{k}, x)|S(\boldsymbol{k}, \sigma)|^2. \qquad (5)$$

As described in Section 2, $\mathrm{D}E_{CS}^{eq}$ can be calculated by the energy change caused by deformation of the *pure* bulk elements Al and fcc Zn in well-defined directions for a common lattice constant a. Consequently $\mathrm{D}E_{CS}^{eq}$, and therefore $E_{CS}(\sigma)$, does not include information about the strength of chemical interactions between Al and Zn atoms, but is a function of composition x and direction $\hat{k}$ only. Precipitate shapes calculated by considering only $E_{CS}(\sigma)$ will therefore reflect the elastic properties of the alloy system. Second, we present the case where non-strain (pair and multibody) interactions to come into play:

$$E_{chem}(\sigma) = \sum_{\boldsymbol{k}} J_{pair}(\boldsymbol{k})|S(\boldsymbol{k}, \sigma)|^2 + \sum_{f}^{MB} D_f J_f \bar{P}_f(\sigma). \quad (6)$$

This part includes all of the information about strength and importance of different chemical interactions characterized by effective cluster interactions J_{pair} and J_f. It does not consider the energy necessary to maintain coherency between the Al and fcc Zn matrix caused by the lattice misfit; i.e., the precipitate is able to maintain coherency with the Al matrix for any arbitrary precipitate size. Precipitate shapes calculated by considering only $E_{chem}(\sigma)$ will therefore reflect the properties of the chemical interactions in Al–Zn. Naturally, this separation is not unique, but, as we shall see, it allows us to discuss and understand by which energetical factors the precipitate shape is controlled. It should be emphasized that an analogous decomposition of precipitate *shapes* corresponding to the two defined energy parts of the Hamiltonian is not possible because, unlike the energies, geometrical shapes are *not* additive.

For the following, a fixed precipitate size ($N_{Zn} = 11{,}656$) was chosen. The Monte-Carlo cell consisted of $60 \times 60 \times 60 = 216{,}000$ atoms which defines the considered alloy as $Al_{0.946}Zn_{0.054}$. The MC annealing process was made for three different cases: (a) using only the consituent strain energy E_{CS}, (b) using the chemical

cess. Unlike the simulations leading to Fig. 9, the decomposition of the energy was always made *after* the MC simulation. The resulting energy curves for the total Hamiltonian ΔH, the chemical energy E_{chem} and the strain energy E_{CS} as function of temperature are shown in Fig. 10. Since the energy was separated after the simulation, for each temperature, the sum of chemical and strain energy must be equal to the total energy ΔH per Zn atom. We observe the following:

1. at high temperatures (> 150 K) the contribution of the chemical energy to the total energy is larger than the contribution of the strain energy, while the opposite is true for lower temperatures (, 150 K); and
2. while the chemical energy decreases strongly with decreasing temperature, the strain energy is nearly temperature-independent.

The temperature dependence of the two energy components becomes more obvious if we separate them into *temperature-dependent* and *temperature-independent* parts. For this, the CE Hamiltonian is written as

$$\Delta H = E_{chem}(N, T_C) + [E_{chem}(N, T) - E_{chem}(N, T_C)] + E_{CS}(N, 0) + [E_{CS}(N, T) - E_{CS}(N, 0)]. \quad (7)$$

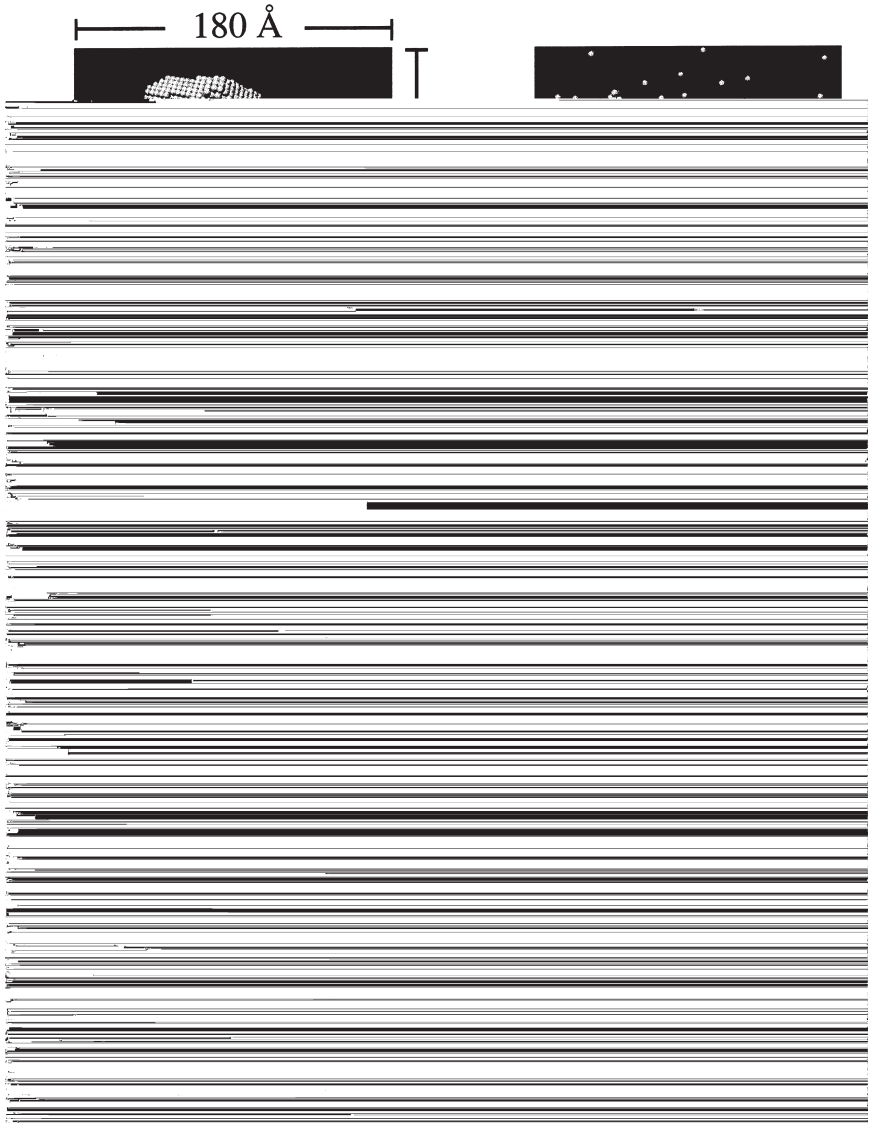

Fig. 10. Dependence of energy ΔH on temperature for a given precipitate size (N_{Zn} = 11,656). After annealing, the energy was decomposed into strain E_{CS} and chemical E_{chem} parts. While for temperatures higher than ~ 150 K the contribution of the chemical part to the total energy is larger than that of the strain part, the opposite is true for lower temperatures. For $T \rightarrow T_C$ and $T \rightarrow 0$ K the resulting precipitate shapes are shown (only Zn atoms are shown).

Here, $E_{\mathrm{chem}}(N, T$

The dependence of the shape on the size at $T = 0$ K can already be found by calculating energies for perfectly ordered model precipitates. We used an ideal spherical precipitate and hexagons with c/a ratios of 0.8, 0.5 and 0.35 for our calculations. These four model precipitates already give qualitatively, via Monte-Carlo simulations, the observed size versus shape relation: namely, a decreasing c/a ratio with increasing precipitate size.

The separation of the cluster expansion Hamiltonian into chemical and strain energy allows a deeper view inside the energetically controlled size versus shape relation. Monte-Carlo simulations only taking the chemical and strain energy into account lead, for $T = 0$ K, to different characteristic shapes for both energy parts: while the strain energy is platelet-stabilizing, the chemical part leads to a more spherical shape. Using this separation also for finite temperatures, it turns out that the shape versus size versus temperature relation for a given precipitate size is controlled by two different factors:

1. competition between strain and chemical energy—the chemical energy dominates over the strain part for higher temperatures, and the opposite is true for lower temperatures; and
2. temperature dependence of chemical energy—while the strain energy is nearly constant as a function of temperature, the chemical energy decreases strongly with decreasing temperature.

Since our model is parameter-free, the excellent agreement demonstrates the ability to predict precipitate shapes and sizes even without carrying out experiments.

Acknowledgements—The work at NREL was supported by the Office of Science, Basic Energy Science, Material Science Division, US Department of Energy, under Contract No. DE-AC36-99-GO10337.

REFERENCES

1. Guinier, A., *Solid State Phys.*, 1959, **9**, 293.
2. Cohen, J. B., *Solid State Phys.*, 1986, **39**, 131.
3. Khachaturyan, A. G., *Theory of Structural Transformations in Solids*. John Wiley, New York, 1983.
4. Gerold, V., *Scripta Metall.*, 1988, **22**, 927.
5. Mattila, T., Wang, L. -W. and Zunger, A., *Phys. Rev. B*, 1999, **59**, 15270.
6. Zunger, A. and Mahajan, S., chapter 19, in *Material, Properties, and Preparation*, ed. S. Mahajan, Handbook of Semiconductors, Vol. 3B, North Holland, New York, 1994, p. 1399.
7. Hansen, M., *Consitution of Binary Alloys*., McGraw-Hill, New York, 1958.
8. Hultgren, R., Desai, P. D., Hawkins, D. T., Gleiser, M. and Kelley, K. K., *Selected Values of the Thermodynamic Properties of Binary Alloys*., American Society for Metals, Metals Park, OH, 1973.
9. Massalski, T. B., in *Binary Alloy Phase Diagrams*, eds J. L. Murray, L. H. Bennett and H. Baker, American Society for Metals, Metals Park, OH, 1986.
10. Murray, J. L., *Bull. All. Ph. Diagr.*, 1983, **4**, 55.
11. Hatch, J. E., *Aluminum: Properties and Physical Metallurgy*. American Society for Metals, Metals Park, OH, 1998.
12. Laslaz, G. and Guyot, P., *Acta metall.*, 1977, **25**, 277.
13. Deguercy, J., Denanot, M. F., Fumeron, M., Guillot, J. P. and Caisso, J., *Acta metall.*, 1982, **30**, 1921.
14. Ramlau, R. and Löffler, H., *Phys. Stat. Sol. (a)*, 1981, **68**, 531.
15. Ramlau, R. and Löffler, H., *Phys. Stat. Sol. (a)*, 1983, **79**, 141.
16. Bubeck, E., Gerold, V. and Kostorz, G., *Cryst. Res. Technol.*, 1985, **20**, 97.
17. Hübner, G., Löffler, H. and Wendrock, G., *Cryst. Res. Technol.*, 1986, **21**, 8.
18. Gerold, V., Siebke, W. and Tempus, G., *Phys. Stat. Sol. (a)*, 1987, **104**, 213.
19. Guilarducci de Salva, A., P Simon, J., Livet, F. and Guyot, P., *Scripta metall.*, 1987, **21**, 1061.
, 1987, **21**